Non-Newtonian Flow Behavior of Diblock Copolymer Micelles: Shear-Thinning in a Nonentangling Matrix

Hiroshi Watanabe,*,† Ming-Long Yao,‡ Tomohiro Sato,† and Kunihiro Osaki†

Institute for Chemical Research, Kyoto University, Uji, Kyoto 611, Japan, and Rheometric Scientific, F.E., 2-19-6 Yanagibashi, Taito-ku, Tokyo 111, Japan

Received December 18, 1996; Revised Manuscript Received June 4, 1997[⊗]

ABSTRACT: Non-Newtonian flow behavior was examined for a styrene−isoprene (SI) diblock copolymer (M_S = 13.9K, M_I = 28.8K) in a low-M homopolyisoprene matrix (I-4; M = 4.1K) at −20 °C where the copolymer formed spherical micelles with glassy S cores and soft I corona. Those micelles (15 wt % in the system) were isotropically dispersed in the I-4 matrix at equilibrium, and the corona blocks were entangled neither among themselves nor with the short matrix. The viscosity η of this *micellar dispersion* exhibited two-step shear-thinning behavior. Molecular origin of this behavior was examined in relation to previously investigated linear and nonlinear relaxational features of the SI micelles. In the linear regime (for small strain), the micelles exhibited fast and slow relaxation processes. The fast process was due to the relaxation of the micellar corona, while the slow process was related to the thermodynamic (Brownian) stress that reflected a strain-induced anisotropy in the spatial distribution of the micelles. This stress relaxed when the isotropic distribution was recovered *via* diffusion of the micelles. For large step-strains γ, the micelles exhibit nonlinear damping of the relaxation modulus. Modest damping for the fast process reflected changes in the conformation (shrinkage) of the corona blocks, and the much stronger damping for the slow process was related to a γ-insensitivity of the anisotropy of the micellar distribution for large γ. These linear and nonlinear relaxation data were utilized in a BKZ constitutive equation to calculate the viscosity η_{BKZ}. η_{BKZ} agreed well with the η data. This agreement indicated that the shear-thinning behavior of the SI micelles had a molecular origin identical to those for the nonlinear damping for the fast and slow processes. On the basis of this result, similarities and differences were discussed for the micellar dispersion and a silica suspension, the latter containing randomly dispersed silica particles at the quiescent state and exhibiting the thinning and thickening behavior at low and high shear rates.

I. Background

Styrene−butadiene (SB) and styrene−isoprene (SI) diblock copolymers exhibit a wide variety of rheological and structural features in selective solvents. In diene-selective solvents of monomeric sizes (e.g., *n*-tetradecane) at low temperatures, the copolymers with relatively small S content from spherical micelles with glassy S cores and solvated B/I corona. In concentrated solutions where these micelles overlap at their coronas, the corona blocks are osmotically required to maintain a uniform concentration in the matrix phase (containing solvent molecules and corona segments). This requirement forces the corona blocks to take mutually constrained conformations having small entropy, and the micelles are arranged on cubic lattices so as to minimize this *osmotic constraint* for the corona conformation.[1−4] This lattice structure governs rheological responses of the micellar solutions at long time scales:[1−4] The lattice deforms elastically and behaves as a solid for stresses (σ) smaller than the lattice strength (yield stress σ_y), while it flows plastically and behaves as a liquid for $\sigma > \sigma_y$.

For SB micelles in matrices of low-M homopolybutadiene (hB) chemically identical to the corona, the hB chains maintain the uniform B segment distribution in the matrix irrespective of the corona conformation. In other words, the hB chains screen the osmotic constraint for the corona B block conformation, thereby allowing those blocks to take a randomized conformation without paying an osmotic penalty.[3,4] Thus, in the short hB matrices, the driving force of the lattice formation vanishes and the micelles are randomly dispersed (unless they are highly concentrated and the hB chains only partially screen the osmotic constraint).[3,4] Consequently, such SB micellar dispersions exhibit no plasticity and relax viscoelastically.[3−8] Similar rheological features were found also for SI micelles randomly dispersed in homopolyisoprene (hI) matrices.[9,10]

For those SB/SI micelles in short *nonentangling* hB/hI matrices, the viscoelastic relaxation proceeds *via* fast and slow processes.[7,9,10] From examination of the relaxation time and mode distribution in the linear regime, the fast process is attributed to the starlike relaxation of individual corona blocks (that is significantly retarded by impenetrable S cores when neighboring micelles are entangled through their corona).[7,9] On the other hand, examination of the relaxation time enabled us to relate the slow process to the micellar diffusion:[7,9] At equilibrium, the micelles are randomly and isotropically distributed in the system to have the maximum placement entropy. A strain distorts this distribution to decrease the entropy and raises a thermodynamic (*Brownian*) stress, and this stress relaxes on recovery of the isotropic distribution *via* the micellar diffusion. For large step-strains, the fast and slow processes exhibit nonlinear damping that reflects the respective relaxation mechanisms in the linear regime.[10]

Here, we note striking similarities between the micellar systems and suspensions of solid particles in viscous media. The quasi-static, elasto-plastic feature of the micellar lattice systems is quite similar to that of *colloidal crystals* of charged particles.[1,11−13] Under fast flow, the micellar lattices[14,15] exhibit characteristic rheological and structural changes that are again

* To whom correspondence should be addressed.
† Kyoto University.
‡ Rheometric Scientific, F.E.
⊗ Abstract published in *Advance ACS Abstracts,* September 1, 1997.

S0024-9297(96)01867-0 CCC: $14.00

similar to the changes seen for the colloidal crystals:[11−13,16−19] These two types of lattice systems commonly exhibit shear-thickening due to lattice melting at very high shear rates, shear-thinning and enhancement of the lattice order at lower shear rates, and for some cases hysteresis of the stress resulting from changes in the lattice type (e.g., from faulted lattices to polycrystalline structure).

Similarities are found also for the micellar dispersions and so-called *hard-sphere suspensions* that contain small solid particles having a short-ranged, hard-core repulsive interaction (no long-ranged repulsion/attraction). These particles, randomly distributed in the systems at the quiescent state, exhibit linear viscoelastic relaxation of the Brownian stress[20−24] as well as nonlinear damping of the relaxation modulus[24] that are similar, in nature, to those for the slow process of the micellar dispersion.

The suspensions also exhibit characteristic nonlinear features under *steady flow*. Extensive experiments[24−35] and Stokesian dynamic simulations[36−39] revealed the shear-thinning and shear-thickening of the suspension viscosities, the former often attributed to flow-induced ordering (string/layer formation) of the particles and the latter, to disruption of those ordered structures and formation of nonpermanent, dynamic clusters. However, for some cases, the string/layer formation is not clearly detected in the shear-thinning regime.[28,31,35] The thinning for these cases is related to decreases of the Brownian contribution to the viscosity with increasing shear rates.[24,34,35,38]

On the basis of the above background, it is of our particular interest to compare the flow behavior of the micellar dispersion with that of the hard-sphere suspension. From this point of view, we have examined the steady as well as transient flow behavior for a SI micellar dispersion of known relaxational features.[9,10] This paper presents the results, focusing its attention to similarities and differences between the micellar dispersion and a hard-sphere suspension of silica particles.[24]

II. Experimental Section

For a 15 wt % blend of a monodisperse styrene−isoprene diblock copolymer (SI 14-29; M_S = 13.9K, M_I = 28.8K)[9] in a short, nonentangling homopolyisoprene matrix (I-4; M = 4.1K),[9] steady and transient flow behavior was examined at −20 °C with a laboratory rheometer (ARES, Rheometrics). Spherical SI micelles with glassy S cores and soft I corona were isotropically and randomly dispersed in the I-4 matrix at the quiescent state. In the matrix phase, the corona I blocks had a volume fraction $\phi_I \cong 0.11$ and a reduced molecular weight $M_{r,I} = \phi_I M_I \cong 3.2$K. Since this $M_{r,I}$ is smaller than the entanglement molecular weight for bulk polyisoprene, M_e = 5K, the I blocks in the blend are entangled neither among themselves nor with the short I-4 matrix.[9]

In the 15 wt % SI micellar dispersion, the S cores have a volume fraction $\phi_c \cong 0.043$. Each S core has a radius $r_S \cong 80$ Å[9] and is composed of $N_m \cong 100$ S blocks. A *nominal* volume fraction of the micelles in the system, ϕ_m, is calculated from r_S, N_m, and the end-to-end distance R_I of the I blocks (corona thickness). ϕ_m is evaluated to be 0.87 if the I blocks have the unperturbed size, $R_{I,\theta} \cong 140$ Å.[9] In reality, the I blocks should have $R_I > R_{I,\theta}$ because of the repulsion from the S core,[9] and ϕ_m is larger than unity. These nominal ϕ_m values are too large to be realized for hard spheres, meaning that the SI micelles overlap to some extent at their corona. (Despite this partial overlapping, the I blocks have $M_{r,I} < M_e$ and are in the nonentangled state.)

For suspensions in general, rheological behavior is dependent on the particle content. Since our SI micelles have soft and penetrable coronas, their *rheologically effective* volume fraction ϕ_{eff} should be smaller than the nominal ϕ_m explained above. However, ϕ_{eff} should be significantly larger than ϕ_c, and the micelles can be regarded as particles that are considerably crowded in the system. From this point of view, non-Newtonian flow behavior was compared for the micellar dispersion and a concentrated silica suspension ($\phi_{eff} = 0.53$)[24] exhibiting nearly the same magnitude of nonlinear damping.

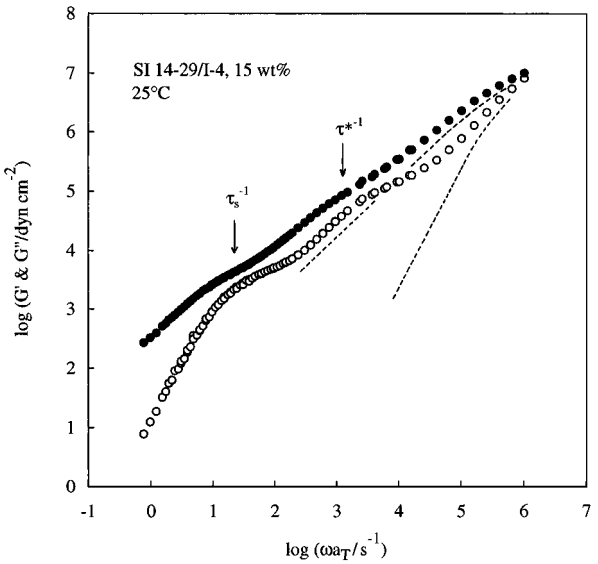

Figure 1. Frequency (ω) dependence of the storage and loss moduli G' and G'' of the 15 wt % SI 14-29/I-4 micellar dispersion reduced at 25 °C.[9] The dashed curves indicate the behavior of the I-4 matrix. The arrows indicate characteristic frequencies for the fast and slow relaxation processes of the micelles.

For the 15 wt % SI micellar dispersion, linear dynamic moduli G^* and nonlinear relaxation modulus $G(t,\gamma)$ were fully characterized in our previous work.[9,10] Growing and decaying strseses $\sigma_+(t,\dot\gamma)$ and $\sigma_-(t,\dot\gamma)$ on start-up and cessation of flow at shear rate $\dot\gamma$ as well as the steady stress $\sigma_s(\dot\gamma)$ ($=\sigma_+(\infty,\dot\gamma)$) were measured in this study in a cone-and-plate geometry of radius = 2.5 cm and gap-angle = 0.04 rad. From these stress data, the viscosity growth and decay functions $\eta_+(t,\dot\gamma)$ and $\eta_-(t,\dot\gamma)$ and the steady state viscosity $\eta(\dot\gamma)$ were evaluated as

$$\eta_+(t,\dot\gamma) = \sigma_+(t,\dot\gamma)/\dot\gamma, \quad \eta_-(t,\dot\gamma) = \sigma_-(t,\dot\gamma)/\dot\gamma, \quad \eta(\dot\gamma) = \sigma_s(\dot\gamma)/\dot\gamma \quad (1)$$

These viscosities, measured for $0.01 \le \dot\gamma\ (s^{-1}) \le 25$ at −20 °C, were reduced to a reference temperature T_r = 25 °C previously used for the G^* and $G(t,\gamma)$ data.[9,10] (The time−temperature superposition was valid for the SI 14-29 micellar dispersion,[9,10] and the shift factor a_T obtained for G^* was used for this reduction.)

III. Results

III-1. Overview for Relaxation Behavior. For convenience for later analyses of the viscosity data, we here summarize linear and nonlinear relaxational features of the SI 14-29/I-4 micellar dispersion at 25 °C. Figure 1 shows master curves of linear viscoelastic moduli G' and G'',[9] and Figure 2 demonstrates nonlinear relaxation moduli $G(t,\gamma)$ obtained for step-strains γ.[10] (The $G(t,\gamma)$ data, measured at −25, 5, and 25 °C, were reduced at 25 °C.[10])

In Figure 1, the dotted curves indicate the behavior of the I-4 matrix. This matrix has fully relaxed at frequencies $\omega a_T < 10^4\ s^{-1}$. At those low ωa_T values, the dispersion exhibits two-step relaxation that is exclusively attributed to the relaxation of the SI micelles having glassy S cores and soft I coronas. The fast relaxation process corresponds to relaxation of individual corona blocks while the slow process is attribut-

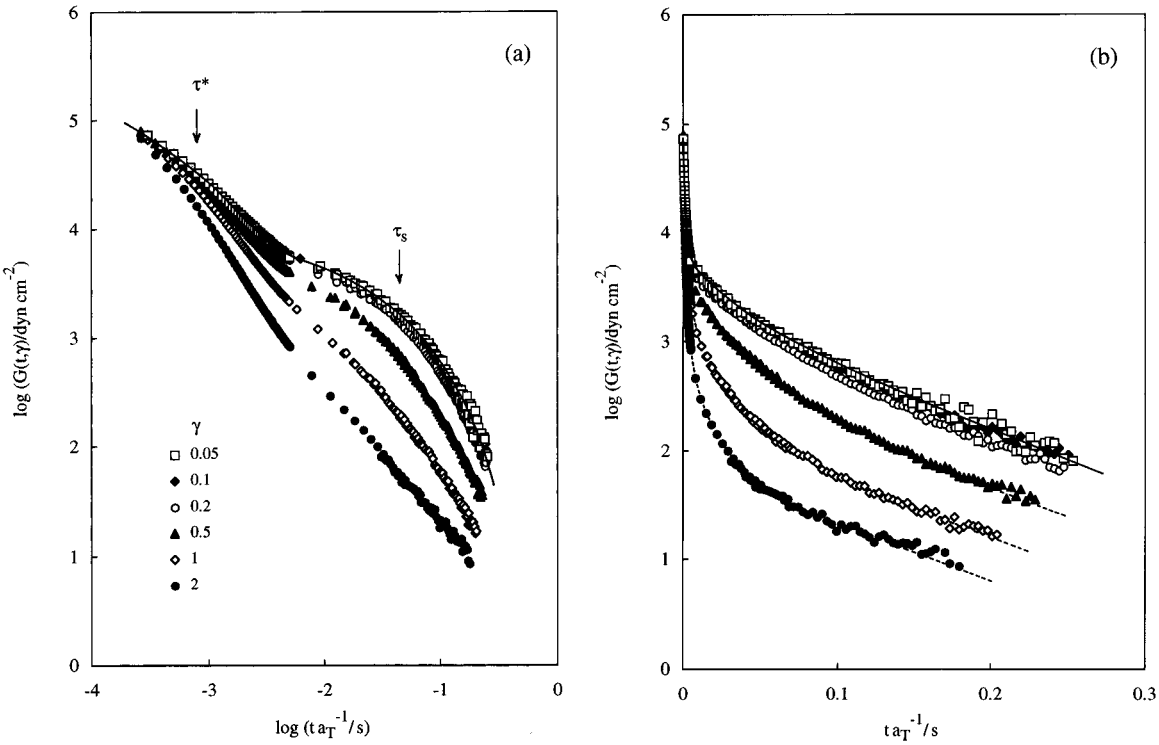

Figure 2. Nonlinear relaxation modulus $G(t,\gamma)$ of the 15 wt % SI 14-29/I-4 micellar dispersion.[10] The data measured at −25, 5, and 25 °C are reduced at 25 °C. In both parts a and b, the solid curves represent the linear relaxation modulus of the SI micelles evaluated from the G^* data.[10] The arrows in part a indicate relaxation times for the fast and slow processes of the micelles determined in the linear regime.

Table 1. Fitting Parameters[a] for Linear Relaxation Moduli for Fast and Slow Processes of the 15 wt % SI 14-29/I-4 Micellar Dispersion at 25 °C

p	$10^{-3}g_p$/dyn cm^{-2}	$10^{-2}\lambda_p$/s^{-1}
	For $G_f(t)$ for the Fast Process[49]	
1	44.5	10.9
2	7.5	14.4
3	133	61.4
4	147	411
5	87.8	2619
	For $G_s(t)$ for the Slow Process	
1	2.11	0.13
2	3.19	0.41
3	2.29	1.82

[a] $G_x(t) = \sum_p g_p \exp(-\lambda_p t)$; x = f, s.

able to relaxation of anisotropy of the micellar distribution (decay of the Brownian stress) due to the micellar diffusion.[9,10] The arrows indicate characteristic frequencies τ^{*-1} and τ_s^{-1} for the fast and slow processes, with τ^* (=7.9 × 10^{-4} s) and τ_s (=4.5 × 10^{-2} s) being the relaxation times of respective processes.[9]

The I-4 matrix has relaxed at the time scales examined in Figure 2. Thus the relaxation seen there is exclusively attributed to the relaxation of the SI 14-29 micelles. In both parts a and b, the solid curves indicate a linear relaxation modulus $G(t)$ of the micelles evaluated from the G^* data.[10] For $\gamma \leq 0.1$, $G(t,\gamma)$ agrees with $G(t)$ and linear relaxation behavior prevails. For larger γ, $G(t,\gamma)$ exhibits nonlinear damping that is much stronger for the slow process. In the semilogarithmic plots (Figure 2b), we note that log $G(t,\gamma)$ decays linearly with time at $t > \tau_s$ and the slope of this linear portion, giving the terminal relaxation rate for the slow process, is insensitive to γ in the range of γ examined.

These $G(t,\gamma)$ data were decomposed into the relaxation moduli $G_f(t,\gamma)$ and $G_s(t,\gamma)$ for the fast and slow processes, and the validity of the time−strain separability[40−44] was examined for respective processes:[10] At $t > 6\tau^*$ where the fast process is completed, the $G(t,\gamma)$ data coincide with $G_s(t,\gamma)$. Fitting those $G_s(t,\gamma)$ data at $t > 6\tau^*$ with an empirical equation composed of exponentially decaying terms (cf. Table 1 shown later) and extrapolating this equation to $t = 0$, we evaluated $G_s(t,\gamma)$ at $t < 6\tau^*$ and $G_f(t,\gamma) = G(t,\gamma) - G_s(t,\gamma)$. $G_f(t,\gamma)$ and $G_s(t,\gamma)$ were successfully separated with this procedure.[10] As an example, Figure 3 demonstrates $G_f(t)$ and $G_s(t)$ obtained in the *linear* viscoelastic regime ($\gamma = 0.05$). These $G_f(t)$ and $G_s(t)$ data are later utilized in analyses of the viscosity data.

The $G_f(t,\gamma)$ and $G_s(t,\gamma)$ data obtained for $\gamma \leq 2$ satisfied the time−strain separability at respective terminal regimes,[10]

$$G_f(t,\gamma) = h_f(\gamma)G_f(t),\ G_s(t,\gamma) = h_s(\gamma)G_s(t) \qquad (2)$$

Here, $h_f(\gamma)$ and $h_s(\gamma)$ are the damping functions for the fast and slow relaxation processes. Figure 4 shows these functions for the SI 14-29/I-4 micellar dispersion (large symbols). For comparison, Figure 4 also shows the damping function $h_c(\gamma)$ for entangled homopolymer chains[41−43] (small circles) and $h_{sus}(\gamma)$ for a hard-sphere suspension of silica particles[24] (small squares). Those particles had a radius r_p = 400 Å and an effective volume fraction $\phi_{eff} = 0.53$, and were dispersed in a 2.27/1 (wt/wt) mixture of ethylene glycol and glycerol (EG/Gly) to exhibit relaxation of the Brownian stress.[24]

As noted in Figure 4, $h_f(\gamma)$ of the SI 14-29 micelles agrees well with $h_c(\gamma)$ of homopolymer chains. These chains, stretched by large step-strains, exhibit nonlinear damping due to shrinkage.[43−45] Thus, the damping for the fast process is also attributed to the motion (shrinkage) of individual corona blocks,[10,45] being in harmony with the molecular assignment for this process in the linear regime.

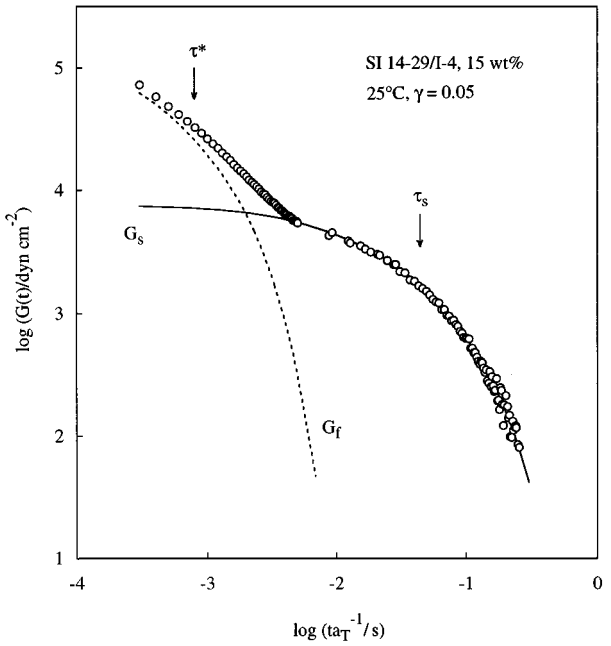

Figure 3. Decomposition of the relaxation modulus $G(t,\gamma)$ of the 15 wt % SI 14-29 micelles at 25 °C into the moduli G_f and G_s for the fast and slow relaxation processes.[10] For $\gamma = 0.05$, $G(t,\gamma)$ coincides with the linear $G(t)$.

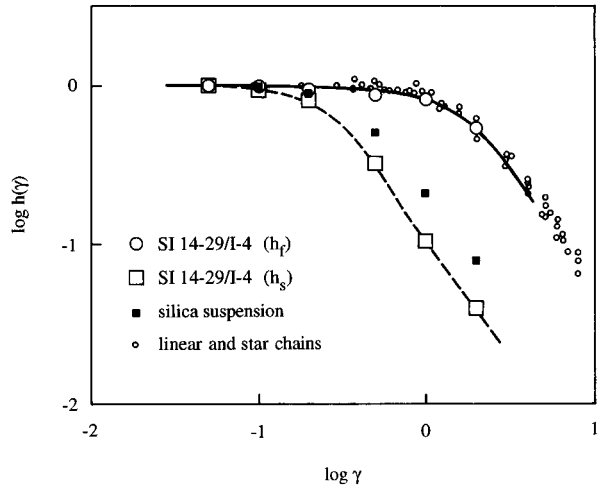

Figure 4. γ dependence of the damping functions $h_f(\gamma)$ and $h_s(\gamma)$ for the fast and slow relaxation processes of the 15 wt % SI 14-29/I-4 micellar dispersion (large circles and squares).[10] The solid and dashed curves indicate empirical fitting equations for $h_f(\gamma)$ and $h_s(\gamma)$. The small, filled squares indicate $h(\gamma)$ for a hard-sphere suspension of silica particles at −40 °C,[24] and the small circles show $h(\gamma)$ for entangled linear and/or star polystyrene chains.[41−43]

In Figure 4, we also note that $h_s(\gamma)$ of the SI 14-29 micelle is close to $h_{sus}(\gamma)$ of the silica suspension. This result suggests a similarity in the nonlinear damping mechanisms for the micelles (at long time scales) and the suspension. For the suspension, the damping is related to the molecular origin of the Brownian stress σ_B, the strain-induced anisotropy in the spatial distribution of the particles:[24] The anisotropy increases in proportion to γ for sufficiently small γ to raise the linear viscoelastic $\sigma_B \propto \gamma$. However, for large γ, the anisotropy becomes insensitive to γ, resulting in nonlinear damping (decrease of σ_B/γ).[24] The slow relaxation process of the SI micelles should have the same damping mechanism that reflects the γ-insensitivity of the micellar distribution for large γ.[46]

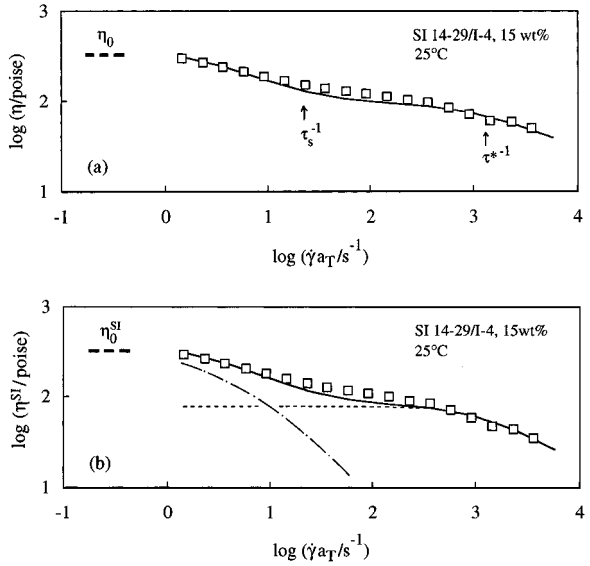

Figure 5. $\dot\gamma$ dependence of the steady state viscosity $\eta(\dot\gamma)$ of the 15 wt % SI 14-29/I-4 micellar dispersion at 25 °C (part a). The $\eta(\dot\gamma)$ data measured at −20 °C were reduced at 25 °C. Part b shows the dependence of the viscosity $\eta^{SI}(\dot\gamma)$ of the SI micelles (obtained by subtracting the matrix contribution from η). In parts a and b, the solid curves indicate the BKZ predictions for η and η^{SI} calculated from the $G_x(t)$ and $h_x(\gamma)$ data (x = f, s). In part b, the dotted and dash−dot curves indicate the BKZ predictions for the contributions of the fast and slow processes to η^{SI}.

III-2. Steady Flow Behavior. For the SI 14-29/I-4 micellar dispersion, $\dot\gamma$ dependence of the steady state viscosity $\eta(\dot\gamma)$ is shown in Figure 5. (The $\eta(\dot\gamma)$ data measured at −20 °C were reduced to 25 °C.) The horizontal dashed line indicates the zero-shear viscosity η_0, and the arrows represent the characteristic frequencies τ^{*-1} and τ_s^{-1} for the fast and slow relaxation processes of the SI micelles in the linear regime. The solid, dash−dot, and dotted curves indicate viscosities calculated from a BKZ (Bernstein−Kearsley−Zapas) constitutive equation[47,48] explained later.

Figure 5a demonstrates that $\eta(\dot\gamma)$ decreases from η_0 and exhibits two-step shear-thinning with increasing $\dot\gamma$. As can be noted from Figure 1, the I-4 matrix behaves as a Newtonian liquid at $\dot\gamma$ examined ($\dot\gamma a_T < 10^4$ s^{-1}). Thus the thinning of $\eta(\dot\gamma)$ represents nonlinearities in the steady flow behavior of the SI micelles. Specifically, the thinning at low $\dot\gamma$ (around τ_s^{-1}) is related to nonlinearities for the slow, micellar diffusion process while that at high $\dot\gamma$ (around τ^{*-1}) reflects nonlinearities for the fast, corona relaxation process. (Since the S cores of the SI micelles are glassy and rigid at −20 °C where the $\eta(\dot\gamma)$ data were measured, the thinning is not due to deformation/rupture of the S cores.) These nonlinearities are most clearly examined for the micellar contribution η^{SI} to the viscosity. The η^{SI} data obtained by subtracting the matrix contribution from the η data are shown in Fugure 5b.

For comparison with the thinning behavior of the 15 wt % SI 14-29 micellar dispersion, the steady flow behavior of the silica suspension ($\phi_{eff} = 0.53$)[24] is shown in Figure 6. This suspension and the micellar dispersion exhibit nearly the same magnitude of nonlinear damping against step-strains ($h_{sus} \cong h_s$; cf. Figure 4). Thus, the micellar dispersion and silica suspension are expected to exhibit similar non-Newtonian flow behavior if the former effectively behaves as a hard-sphere suspension under any type of deformation (i.e., step-strain and steady flow).

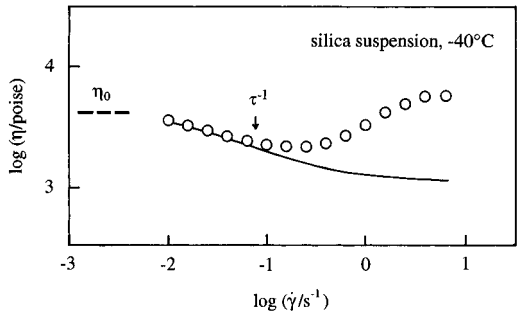

Figure 6. $\dot{\gamma}$ dependence of the steady state viscosity $\eta(\dot{\gamma})$ for a hard-sphere suspension of silica particles ($r_p = 400$ Å, $\phi_{eff} = 0.53$) in an EG/Gly mixture at −40 °C.[24] The solid curve indicates the BKZ prediction calculated from the $G(t)$ and $h(\gamma)$ data.[24]

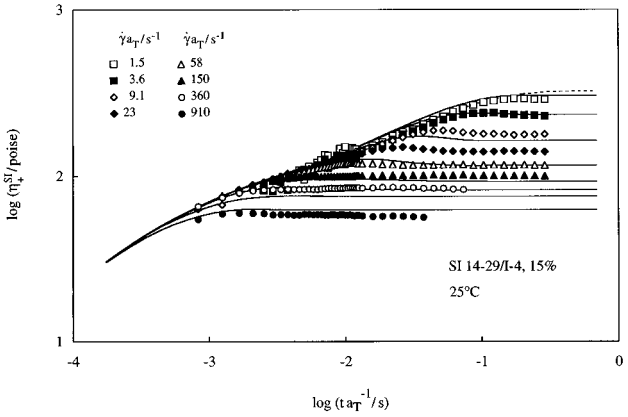

Figure 7. Plots of the viscosity growth function $\eta_+^{SI}(t,\dot{\gamma})$ for the SI 14-29 micelles at 25 °C against the time after start-up of the shear flow. The $\eta_+^{SI}(t,\dot{\gamma})$ data obtained at −20 °C were reduced at 25 °C. The dotted curve represents the linear growth function $\eta_{+,L}^{SI}(t)$, and the solid curves indicate the BKZ predictions calculated from the $G_x(t)$ and $h_x(\gamma)$ data (x = f, s). $\dot{\gamma}a_T$ (in s^{-1}) for those calculated curves are 1.5, 3.6, 9.1, 23, 58, 150, 360, and 910 from top to bottom.

In Figure 6, the arrow indicates a characteristic shear rate τ^{-1} of the silica suspension, with τ (=13 s) being the terminal relaxation time (corresponding to the particle diffusion process).[24] As similar to the slow process of the SI 14-29 micelles, the suspension exhibits shear-thinning at small $\dot{\gamma} \leq \tau^{-1}$. This result suggests that the molecular origin of the thinning is the same for the micellar dispersion and silica suspension. However, differing from the dispersion, the suspension exhibits shear-thickening at large $\dot{\gamma}$. These similarity and difference are later discussed in relation to the spatial distribution of the micelles under flow.

III-3. Viscosity Growth Behavior. For the SI 14-29/I-4 micellar dispersion, both SI micelles and I-4 matrix have contributions to the viscosity growth function $\eta_+(t,\dot{\gamma})$. The short I-4 matrix exhibits Newtonian behavior to have a constant contribution to η_+ in the time scale examined, $ta_T^{-1} > 10^{-4}$ s. Subtracting this contribution from the η_+ data, we evaluated the viscosity growth function of the SI 14-29 micelles, $\eta_+^{SI}(t,\dot{\gamma})$.

Figure 7 shows the time evolution of $\eta_+^{SI}(t,\dot{\gamma})$ at 25 °C. To avoid heavy overlapping of the data points, the data are shown for representative $\dot{\gamma}$. The solid curves indicate the nonlinear growth functions calculated with a BKZ constitutive equation explained later. The dotted curve indicates a growth function $\eta_{+,L}^{SI}(t)$ in the linear regime calculated from the relationship[40]

$$\eta_{+,L}^{SI}(t) = \int_0^t G(t')\,dt' \tag{3}$$

Here, $G(t) = G_f(t) + G_s(t)$ is the linear relaxation modulus of the SI micelles (cf. Figure 3).

As seen in Figure 7, the linear $\eta_{+,L}^{SI}(t)$ increases with t in two steps. The increase of $\eta_{+,L}^{SI}(t)$ at small t is dominated by the contribution from the fast relaxation process of the SI 14-29 micelles, and the increase at large t reflects the contribution from the slow process. The nonlinear $\eta_+^{SI}(t,\dot{\gamma})$ first follows this $\eta_{+,L}^{SI}(t)$ and increases with t and then deviates downward from $\eta_{+,L}^{SI}(t)$ and approaches the steady state viscosity, $\eta^{SI}(\dot{\gamma})$. This downward deviation characterizes the shear-thinning feature of the SI micelles in a transient state. The deviation takes place separately at short and long time scales, first at long times ($ta_T^{-1} > 10^{-2}$ s) for small $\dot{\gamma}$ and then at short times ($ta_T^{-1} < 10^{-2}$ s) for large $\dot{\gamma}$. As considered for the steady state viscosity (Figure 5), these deviations of $\eta_+^{SI}(t,\dot{\gamma})$ at short and long times are attributed to thinning for the fast and slow processes, respectively. The thinning mechanisms for these processes are later discussed in relation to the mechanism for the hard-sphere suspension of the silica particles.

III-4. Viscosity Decay Behavior. Parts a and b of Figure 8 show double-logarithmic and semilogarithmic plots of the viscosity decay function $\eta_-(t,\dot{\gamma})$ of the SI 14-29/I-4 micellar dispersion against time after cessation of the steady flow. To avoid heavy overlapping of the data points, the data are shown for representative $\dot{\gamma}$. In part a, the solid curves indicate $\eta_-(t,\dot{\gamma})$ calculated from a BKZ constitutive equation explained later, and the dotted curve indicates the decay function $\eta_{-,L}(t)$ in the linear regime calculated from the relationship[40]

$$\eta_{-,L}(t) = \int_t^\infty G(t')\,dt' \tag{4}$$

In part b, the dotted curves smoothly connecting the data points are shown as a guide for the eye.

The stress of the short I-4 matrix relaxes immediately after the cessation of flow (within 10^{-4} s; cf. Figure 1). Thus the $\eta_-(t,\dot{\gamma})$ data seen in Figure 8 represent decay of the stress of the SI 14-29 micelles. As seen there, $\eta_-(t,\dot{\gamma})$ exhibits nonlinear damping that is much more significant at long time scales ($ta_T^{-1} \geq 10^{-2}$ s) where the slow relaxation process of the micelles dominates $\eta_-(t,\dot{\gamma})$. This behavior is similar to the behavior of the nonlinear relaxation modulus $G(t,\gamma)$ (cf. Figure 2). Concerning this fact, Figure 8b shows that log $\eta_-(t,\dot{\gamma})$ decays linearly with t at long time scales, and the slope of this linear portion, giving the terminal relaxation rate of the slow process, is insensitive to $\dot{\gamma}$. This feature is again similar to the feature of $G(t,\gamma)$, the γ-insensitivity of the terminal relaxation rate (Figure 2b).

IV. Discussion

In general, the stress of hard-sphere suspensions has Brownian and hydrodynamic contributions σ_B and σ_H.[13,34,35,38] σ_B reflects the Brownian motion of hydrodynamically interacting particles. Under flow, both σ_B and σ_H increase in proportion to $\dot{\gamma}$ and the Newtonian behavior is observed at sufficiently small $\dot{\gamma}$, while the $\dot{\gamma}$ dependence of either σ_B or σ_H (or both) changes and non-Newtonian behavior prevails for large $\dot{\gamma}$.

For our silica suspension ($\phi_{eff} = 0.53$) having the time-strain separable $G(t,\gamma)$ (cf. Figure 4), we have calculated the viscosities η, η_+, and η_- from a BKZ constitutive equation.[24] In this equation, σ_H was assumed to be

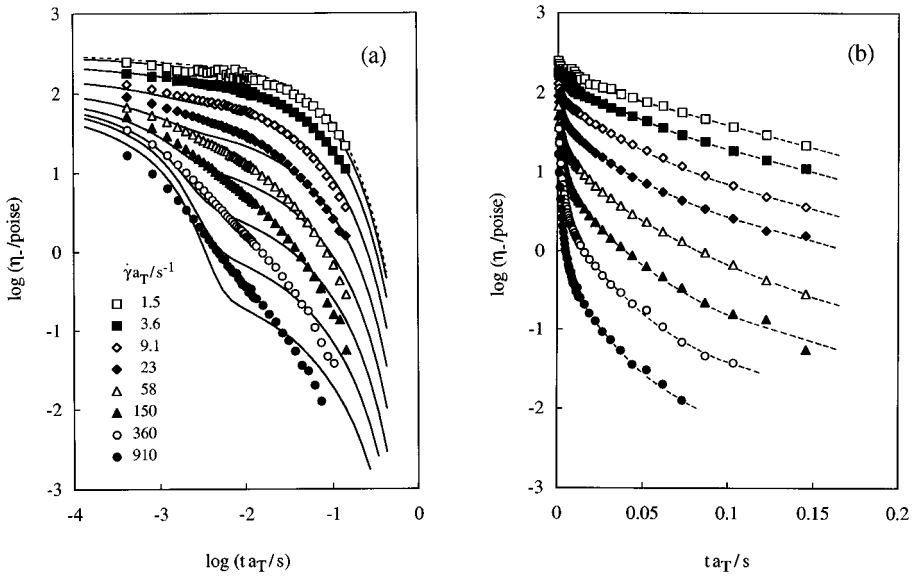

Figure 8. Plots of the viscosity decay function $\eta_-(t,\dot\gamma)$ for the SI 14-29/I-4 micellar dispersion at 25 °C against the time after cessation of the steady shear flow. The $\eta_-(t,\dot\gamma)$ data obtained at −20 °C were reduced at 25 °C. In the time scale examined, the I-4 matrix has fully relaxed and the decay of $\eta_-(t,\dot\gamma)$ is exclusively attributed to relaxation of the SI micelles. In part a, the dotted curve represents the linear decay function $\eta_{-,L}(t)$ and the thick solid curves indicate the BKZ predictions calculated from the $G_x(t)$ and $h_x(\gamma)$ data (x = f, s). $\dot\gamma a_T$ (in s^{-1}) for those calculated curves are 1.5, 3.6, 9.1, 23, 58, 150, 360, and 910 from top to bottom. In part b, the dotted curves smoothly connecting the data points are shown as a guide for the eye.

proportional to $\dot\gamma$ and identical to that in the Newtonian regime while the nonlinearity of σ_B was expressed in terms of the stress relaxation data ($G(t)$ and $h(\gamma)$ data) obtained against *step-strains*.[24] Thus, the nonlinearities under flow (thinning/thickening of the viscosities) should have the ***same*** molecular origin as the nonlinearity against step-strains (damping of $G(t,\gamma)$) ***if*** the constitutive equation describes the viscosity data, and *vice versa*. With this strategy for the molecular assignment, we compared the BKZ predictions with the data for the suspension.[24]

In Figure 6, the BKZ prediction for η is shown with the solid curve. The prediction agrees well with the η data in the thinning regime. Similar agreements were found also for η_+ and η_-.[24] These agreements strongly suggest that the thinning of the silica suspension corresponds to the decrease of $\sigma_B/\dot\gamma$ with increasing $\dot\gamma$ and that the thinning mechanism is quite similar to the damping mechanism for $G(t,\gamma)$. From this similarity, we can relate the thinning to the anisotropy in the particle distribution under flow:[24] The anisotropy increases in proportion to $\dot\gamma$ to raise the Newtonian $\sigma_B \propto \dot\gamma$ for sufficiently small $\dot\gamma$, but it becomes insensitive to $\dot\gamma$ for large $\dot\gamma$ to cause the decrease of $\sigma_B/\dot\gamma$. (In an extreme case, the anisotropy may become completely independent of $\dot\gamma$. However, this is not the case for our suspension, which exhibits rather modest thinning of the viscosity.)

Here, we compare the roles of flow and step-strain (continuously and instantaneously applied strains) in the nonlinear rheological phenomena. As seen above, the BKZ equation describes the thinning of the viscosity in terms of the $G(t)$ and $h(\gamma)$ data. This result means that in the damping and thinning phenomena the step-strain and flow play an *equivalent* role of weakening the γ- and/or $\dot\gamma$-dependence of the particle distribution anisotropy. In other words, the thinning of our suspension is not due to structural changes specific to flow (e.g., flow-induced ordering of the particles).[24]

The situation changes in the shear-thickening regime. The BKZ prediction largely deviates from the η data in this regime (cf. Figure 6), meaning that the fast flow is not equivalent to the step-strain. In other words, the flow plays a specific role in the thickening phenomenon. The thickening is attributable to formation of dynamic (nonpermanent) clusters of the particles due to enhanced hydrodynamic interactions under fast flow:[24,34−39] If the particles have no grafted chains on their surfaces (as is the case for our silica particles) a strong, hydrodynamic lubrication force emerges on cluster formation.

Now, we apply the above strategy of molecular assignment to the SI 14-29/I-4 micellar dispersion. $G_f(t,\gamma)$ and $G_s(t,\gamma)$ for the fast and slow relaxation processes of this dispersion obey the time−strain separability with different magnitudes of damping. Thus, for the micellar dispersion, the BKZ equation reads

$$\sigma(t) = \eta_m\dot\gamma(t) + \int_{-\infty}^{t}\frac{\partial G_f(t-t')}{\partial t'}h_f(\gamma_{t;t'})\gamma_{t;t'}\,dt' + \int_{-\infty}^{t}\frac{\partial G_s(t-t')}{\partial t'}h_s(\gamma_{t;t'})\gamma_{t;t'}\,dt' \quad (5)$$

Here, the first term indicates the matrix contribution to the stress $\sigma(t)$ at time t. (The matrix is assumed to be a Newtonian liquid with viscosity η_m.) $\gamma_{t;t'}$ is a strain at time t measured from a past time t', $G_f(t)$ and $G_s(t)$ are the *linear* relaxation moduli for the fast and slow processes (cf. Figure 3), and $h_f(\gamma)$ and $h_s(\gamma)$ are the damping functions for these processes (cf. Figure 4).

For a step-strain, eq 5 leads to the experimentally observed time-strain separability at long time scales, $G(t,\gamma) = G_f(t)h_f(\gamma) + G_s(t)h_s(\gamma)$; cf. eq 2. For the start-up of steady flow at a rate $\dot\gamma$, eq 5 gives

$$\eta_+(t,\dot\gamma) = \eta_m + \eta_+^{SI}(t,\dot\gamma), \quad \eta_+^{SI}(t,\dot\gamma) = \eta_+^{f}(t,\dot\gamma) + \eta_+^{s}(t,\dot\gamma) \quad (6)$$

where the contributions from the fast and slow processes are given by

$$\eta_+^x(t,\dot\gamma) = G_x(t)h_x(\gamma_t)t - \int_0^t \frac{dG_x(t')}{dt'}h_x(\gamma_{t'})t'\,dt' \quad (x = f, s) \tag{7}$$

with $\gamma_t = \dot\gamma \times t$. After cessation of the steady flow, eq 5 leads to

$$\eta_-(t,\dot\gamma) = \eta_-^f(t,\dot\gamma) + \eta_-^s(t,\dot\gamma) \tag{8}$$

with

$$\eta_-^x(t,\dot\gamma) = -\int_0^\infty \frac{\partial G_x(t+t')}{\partial t'}h_x(\gamma_{t'})t'\,dt' \quad (x = f, s) \tag{9}$$

To carry out the integrals in eqs 7 and 9, we used empirical fitting functions: $G_x(t) = \sum_p g_p \exp[-\lambda_p t]$ with x = f and s (shown in Figure 3 with the dotted and solid curves); $h_f(\gamma) = [1 + 0.199\gamma^{2.1}]^{-1}$ and $h_s(\gamma) = [1 + 10\gamma^{2.2}]^{-1}$ ($\gamma \le 0.74$), $h_s(\gamma) = 0.105\gamma^{-1.45}$ ($\gamma > 0.74$) (shown in Figure 4 with the solid and dashed curves). The fitting parameters for the linear moduli are summarized in Table 1.[49]

In Figures 7 and 8a, the BKZ predictions for $\eta_+^{SI}(t,\dot\gamma)$ and $\eta_-(t,\dot\gamma)$ are shown with the solid curves. In Figure 5, the predictions for the steady state viscosities, $\eta(\dot\gamma) = \eta_m + \eta_+^{SI}(\infty,\dot\gamma)$ and $\eta^{SI}(\dot\gamma) = \eta_+^{SI}(\infty,\dot\gamma)$ (the micellar contribution), are shown with the solid curves. The dotted and dash−dot curves in Figure 5b indicate the BKZ predictions for the contributions from the fast and slow processes to η^{SI}, $\eta_+^f(\infty,\dot\gamma)$ and $\eta_+^s(\infty,\dot\gamma)$ (cf. eq 7). The predictions for $\eta(\dot\gamma)$, $\eta^{SI}(\dot\gamma)$, and $\eta_+^{SI}(t,\dot\gamma)$ agree well with data. In particular, Figure 5b demonstrates that the two-step thinning for the SI 14-29 micelles results from a superposition of two thinning processes, one for the fast relaxation (dotted curve) and the other for the slow relaxation (dash−dot curve). The prediction also agrees with the $\eta_-(t,\dot\gamma)$ data reasonably well (Figure 8a), although some differences are seen at high $\dot\gamma$ ($\ge 23\ s^{-1}$).

These agreements strongly suggest that the shear-thinning of the SI 14-29 micelles has the same molecular origin as the nonlinear damping for the fast and slow relaxation processes against large step-strains. Thus, as in the case of homopolymer chains,[44,48] the thinning for the fast process is attributed to changes in the conformation of the corona I blocks under fast flow. On the other hand, the thinning for the slow process is attributable to the $\dot\gamma$-insensitive micellar distribution that results in a decrease of the Brownian contribution to the viscosity ($\sigma_B/\dot\gamma$) with increasing $\dot\gamma$.[50]

The above results demonstrate a similarity in the thinning behavior at small $\dot\gamma$ for the micellar dispersion and silica suspension. However, it should be also emphasized that the silica suspension exhibits significant thickening at large $\dot\gamma$ (Figure 6) while the micellar dispersion does not (Figure 5). This difference appears to reflect an effect of the polymeric corona of the micelles. As explained earlier, the thickening of the silica suspension is attributable to dynamic clustering of bare silica particles that raises a strong lubrication force. For the micelles, the corona appears to disturb the clustering of the micelles (close approach of the S cores). In addition, the corona would largely reduce the lubrication force to suppress the thickening even if the S cores are brought toward contact under very fast flow. These effects of the corona deserve further attention.

Concerning the corona effects, we expect that the high-shear flow behavior of suspensions is sensitive to surface structures (existence of grafted chains) of the particles therein. In fact, Mewis et al.[32] found that a thin graft-layer (with a thickness being 20% of the particle radius) significantly reduces the suspension viscosity at large $\dot\gamma$. This effect of the thin graft-layer appears to be *qualitatively* similar to the corona effects (suppression of thickening), but some *quantitative* difference may exist because the corona of our micelles is considerably thick (the corona thickness > twice of the S core radius.) These similarities and differences can be examined for a series of micelles having the same core size and various corona thickness. Studies for such micelles, possibly providing detailed information for effects of the particle surface on the suspension rheology, are considered as interesting future work.

V. Concluding Remarks

For the 15 wt % SI 14-29/I-4 micellar dispersion exhibiting fast and slow relaxation processes against step-strains, we have observed two-step shear-thinning behavior under steady as well as transient flow. The rheological test utilizing the BKZ constitutive equation has enabled us to attribute the thinning behavior to changes of corona block conformation (thinning for the fast process at large $\dot\gamma$) and to the $\dot\gamma$-insensitive anisotropy of the micellar distribution (thinning for the slow process at relatively small $\dot\gamma$). This molecular origin of the thinning for the slow process is identical to that for the silica suspension, demonstrating the similarities between the micellar dispersion and the hard-sphere suspension. However, these two systems also exhibit a difference: The shear-thickening behavior is not observed for the micellar dispersion. This difference possibly reflects a polymeric character of the micelles having corona blocks. The role of these blocks in suppression of the thickening is an interesting subject to be investigated. Concerning this point, it is also interesting to examine effects of entanglements among the corona blocks of neighboring micelles as well as between the corona blocks and matrix chains on the flow behavior of micellar dispersions. (The SI 14-29/I-4 dispersion examined in this study has neither the corona−corona nor the corona−matrix entanglements.) Results of these studies will be presented in our future papers.

References and Notes

(1) Watanabe, H.; Kotaka, T.; Hashimoto, T.; Shibayama, M.; Kawai, H. *J. Rheol.* **1982**, *26*, 153.
(2) Watanabe, H.; Kotaka, T. *Polym. J.* **1982**, *14*, 739.
(3) Watanabe, H.; Kotaka, T. *J. Rheol.* **1983**, *27*, 223.
(4) Watanabe, H.; Kotaka, T. *Polym. Eng. Rev.* **1984**, *4*, 73.
(5) Watanabe, H.; Kotaka, T. *Macromolecules* **1983**, *16*, 769.
(6) Watanabe, H.; Kotata, T. *Macromolecules* **1984**, *17*, 342.
(7) Watanabe, H.; Sato, T.; Osaki, K. *Macromolecules* **1996**, *29*, 104.
(8) Watanabe, H.; Sato, T.; Osaki, K. *Macromolecules* **1996**, *29*, 113.
(9) Sato, T.; Watanabe, H.; Osaki, K.; Yao, M.-L. *Macromolecules* **1996**, *29*, 3881.
(10) Watanabe, H.; Sato, T.; Osaki, K.; Yao, M.-L. *Macromolecules* **1996**, *29*, 3890.
(11) Chen, L. B.; Zukoski, C. F. *J. Chem. Soc., Faraday Trans.* **1990**, *86*, 2629.
(12) Chen, L. B.; Chow, M. K.; Ackerson, B. J.; Zukoski, C. F. *Langmuir* **1994**, *10*, 2817.
(13) Mackay, M. E.; Kaffashi, B. *J. Colloid Interface Sci.* **1995**, *174*, 117.
(14) Phoon, C. L.; Higgins, J. S.; Allegra, G.; Van Leeuwen, P.; Staples, E. *Proc. R. Soc. London, A* **1993**, *442*, 221.
(15) McConnell, G. A.; Lin, M. Y.; Gast, A. P. *Macromolecules* **1995**, *28*, 6754.
(16) Ackerson, B. J.; Clark, N. A. *Phys. Rev. A* **1984**, *30*, 906.

(17) Ackerson, B. J.; Hayter, J. B.; Clark, N. A.; Cotter, L. *J. Chem. Phys.* **1986**, *84*, 2344.
(18) Chen, L. B.; Zukoski, C. F. *Phys. Rev. Lett.* **1990**, *65*, 44.
(19) Chen, L. B.; Zukoski, C. F.; Ackerson, B. J.; Hanley, H. J. M.; Straty, G. C.; Barker, J.; Glinka, C. J. *Phys. Rev. Lett.* **1992**, *69*, 688.
(20) Mellema, J.; de Kruif, C. G.; Blom, C.; Vrij, A. *Rheol. Acta* **1987**, *26*, 40.
(21) Mellema, J.; van der Werff, J. C.; Blom, C.; de Kruif, C. G. *Phys. Rev. A* **1989**, *39*, 3696.
(22) van der Werff, J. C.; de Kruif, C. G.; Blom, C.; Mellema, J. *Phys. Rev. A* **1989**, *39*, 795.
(23) Shikata, T.; Pearson, D. S. *J. Rheol.* **1994**, *38*, 601.
(24) Watanabe, H.; Yao, M.-L.; Yamagishi, A.; Osaki, K.; Shikata, T.; Niwa, H.; Morishima, Y. *Rheol. Acta* **1996**, *35*, 433.
(25) Hoffman, R. L. *Trans. Soc. Rheol.* **1972**, *16*, 155.
(26) Barnes, H. A. *J. Rheol.* **1989**, *33*, 329.
(27) Ackerson, B. J.; van der Werff, J.; de Kruif, C. G. *Phys. Rev. A* **1988**, *37*, 4819.
(28) Ackerson, B. J. *J. Rheol.* **1990**, *34*, 553.
(29) Boersma, W. H.; Laven, J.; Stein, H. N. *AIChE J.* **1990**, *36*, 321; *J. Colloid Interface Sci.* **1992**, *149*, 10.
(30) Laun, H. M.; Bung, R.; Schmidt, F. *J. Rheol.* **1991**, *35*, 999.
(31) Laun, H. M.; Bung, R.; Hess, S.; Loose, W.; Hess, O.; Hahn, K.; Hädicke, E.; Hingmann, R.; Schmidt, F.; Lindner, P. *J. Rheol.* **1992**, *36*, 743.
(32) Mewis, J.; Frith, W. J.; Strivens, T. A.; Russel, W. B. *AIChE J.* **1989**, *35*, 415.
(33) D'Haene, P.; Mewis, J.; Fuller, G. G. *J. Colloid Interface Sci.* **1993**, *156*, 350.
(34) Bender, J. W.; Wagner, N. J. *J. Colloid Interface Sci.* **1995**, *172*, 171.
(35) Bender, J.; Wagner, N. J. *J. Rheol.* **1996**, *40*, 899.
(36) Bossis, G.; Brady, J. F. *J. Chem. Phys.* **1984**, *80*, 5141.
(37) Brady, J. F.; Bossis, G. *J. Fluid Mech.* **1985**, *155*, 105.
(38) Bossis, G.; Brady, J. F. *J. Chem. Phys.* **1989**, *91*, 1866; Brady, J. F. *J. Chem. Phys.* **1993**, *99*, 567.
(39) Boersma, W. H.; Laven, J.; Stein, H. N. *J. Rheol.* **1995**, *39*, 841.
(40) Ferry, J. D. *Viscoelastic Properties of Polymers*, 3rd ed.; Wiley: New York, 1980.
(41) Osaki, K.; Nishizawa, K.; Kurata, M. *Macromolecules* **1982**, *15*, 1068.
(42) Osaki, K.; Takatori, E.; Kurata, M.; Watanabe, H.; Yoshida, H.; Kotaka, T. *Macromolecules* **1990**, *23*, 4392.
(43) Osaki, K. *Rheol. Acta* **1993**, *32*, 429.
(44) Doi, M.; Edwards, S. F. *The Theory of Polymer Dynamics*, Clarendon: Oxford, England, 1986.
(45) (a) Note that the corona I blocks of the SI 14-29 micelle are nonentangled but exhibit nonlinear damping. This result is related to an important aspect of the damping: In general, polymer chains exhibit the damping against large step-strains whenever the shrinkage (release of the chain stretching) is faster than the rotation (orientational relaxation). In other words, the damping is not intrinsic to entangled chains. In fact, nonentangled homopolymer chains do exhibit the damping[45b] and thus their shrinkage is faster than the rotation. Concerning this fact, we note that the damping is somewhat weaker for those nonentangled chains than for entangled chains.[45b] A similar difference was noted in ref 10 for entangled and nonentangled micellar corona blocks (although the difference is not very significant at $\gamma \leq 2$ examined there). (b) Takatori, E.; Osaki, K.; Kurata, M.; Hirayama, T. *J. Soc. Rheol. Jpn.* **1988**, *16*, 99.
(46) (a) For SI/I-4 micellar dispersions more concentrated than the 15 wt % SI 14-29 dispersion examined here, $h_s(\gamma)$ depends more strongly on γ and becomes close, in magnitude, to the damping function for micellar lattices.[10] This result may be partly related to an excluded volume effect, as also noted for silica suspensions.[46b] (b) Watanabe, H.; Yao, M.-L.; Osaki, K.; Shikata, T.; Niwa, H.; Morishima, Y. Manuscript in preparation for publication in *Rheol. Acta*.
(47) Bernstein, B.; Kearsley, E. A.; Zapas, L. J. *Trans. Soc. Rheol.* **1963**, *7*, 391.
(48) Larson, R. G. *Constitutive Equations for Polymer Melts and Solutions*, Butterworth: Boston, MA, 1988.
(49) For the fast relaxation of the SI 14-29 micelle (15 wt % in the I-4 matrix) and the terminal relaxation of a bulk 4-arm star hI (arm molecular weight $M_a = 36.7$K), excellent agreements were found for plots of reduced moduli $G_r(t) = [M/cRT]G(t)$ against reduced times t/τ.[10] Here, M and c are the molecular weight and concentration for the I-block/star-arm, and $G(t)$ and τ are the linear relaxation modulus and relaxation time ($=G_f(t)$ and τ^* for the micelles; cf. Figure 3). The above agreements indicate that the intensity g_p and rate λ_p for the pth relaxation mode of the SI micelle and star hI satisfy a relationship, $g_{p,SI} = f_g g_{p,star}$ and $\lambda_{p,SI} = f_\lambda \lambda_{p,star}$ with f_g and f_λ being p-independent constants. $g_{p,star}$ and $\lambda_{p,star}$ were successfully determined for $p = 1-5$ from the $G_{star}(t)$ data[10] available in a wide range of t, while $g_{p,SI}$ and $\lambda_{p,SI}$ were obtained only for $p = 1$ and 2 because of a limited t-range for the $G_f(t)$ data of the SI micelle. Thus, utilizing the factors f_g and f_λ determined for $p = 1$ and 2, we evaluated $g_{p,SI}$ and $\lambda_{p,SI}$ for $p = 3-5$ from the $g_{p,star}$ and $\lambda_{p,star}$ data. These $g_{p,SI}$ and $\lambda_{p,SI}$ values (summarized in Table 1) were utilized in the BKZ calculation (eqs 7 and 9).
(50) The stress of the SI micelles have two contributions, the stress σ_I due to individual corona I blocks (the stress associated to the fast process) and the Brownian stress σ_B due to anisotropy of the micellar distribution (the stress associated to the slow process). At low $\dot\gamma$, $\sigma_B/\dot\gamma$ decreases with increasing $\dot\gamma$ but $\sigma_I/\dot\gamma$ remains constant. Thus, at those $\dot\gamma$, the relative contribution of the Brownian stress, $\sigma_B/[\sigma_B + \sigma_I]$, decreases with increasing $\dot\gamma$. Essentially the same situation is found for the silica suspension: In the thinning regime, $\sigma_B/\dot\gamma$ decreases with increasing $\dot\gamma$ but $\sigma_H/\dot\gamma$ remains constant, resulting in a decrease of the relative, Brownian contribution, $\sigma_B/[\sigma_B + \sigma_H]$.

MA961867D